3D printed structures for modeling the Young's modulus of bamboo parenchyma

Acta Biomaterialia xxx (2018) xxx–xxx

Contents lists available at ScienceDirect

Acta Biomaterialia

journal homepage: www.elsevier.com/locate/actabiomat

Full length article

3D printed structures for modeling the Young's modulus of bamboo parenchyma

P.G. Dixon [a], J.T. Muth [b,c], X. Xiao [d], M.A. Skylar-Scott [b,c], J.A. Lewis [b,c], L.J. Gibson [a,*]

[a] Department of Materials Science and Engineering, MIT, Cambridge, MA 02139, United States
[b] John A. Paulson School of Engineering and Applied Science, Harvard University, Cambridge, MA 02138, United States
[c] Wyss Institute for Biologically Inspired Engineering, Harvard University, Boston, MA 02115, United States
[d] Advanced Photon Source, Argonne National Laboratory, Lemont, IL 60439, United States

ARTICLE INFO

Article history:
Received 11 July 2017
Received in revised form 16 December 2017
Accepted 22 December 2017
Available online xxxx

Keywords:
Bamboo
Parenchyma
Micro X-ray computed tomography
3D printing

ABSTRACT

Bamboo is a sustainable, lightweight material that is widely used in structural applications. To fully develop micromechanical models for plants, such as bamboo, the mechanical properties of each individual type of tissue are needed. However, separating individual tissues and testing them mechanically is challenging. Here, we report an alternative approach in which micro X-ray computed tomography (μ-CT) is used to image moso bamboo (*Phyllostachys pubescens*). The acquired images, which correspond to the 3D structure of the parenchyma, are then transformed into physical, albeit larger scale, structures by 3D printing, and their mechanical properties are characterized. The normalized longitudinal Young's moduli of the fabricated structures depend on relative density raised to a power between 2 and 3, suggesting that elastic deformation of the parenchyma cellular structure involves considerable cell wall bending. The mechanical behavior of other biological tissues may also be elucidated using this approach.

Statement of Significance

Bamboo is a lightweight, sustainable engineering material widely used in structural applications. By combining micro X-ray computed tomography and 3D printing, we have produced bamboo parenchyma mimics and characterized their stiffness. Using this approach, we gained insight into bamboo parenchyma tissue mechanics, specifically the cellular geometry's role in longitudinal elasticity.

1. Introduction

Bamboo is widespread in rapidly developing countries such as China, India and Brazil [1,2]. Bamboo culms and woven mats have been used for millennia in traditional construction [3,4]. Recently, there has been increasing interest in structural bamboo products, similar to wood products such as plywood, oriented strand board and laminated beams, that can be fabricated into larger members of a wider range of geometries than whole culms, increasing the potential for bamboo in sustainable construction [5,6].

Bamboo, which is a member of the grass family, has a unique and heterogeneous structure compared to wood [7–9]. Bamboo tissue primarily consists of vascular bundles, made up of stiff, often nearly fully dense sclerenchyma fibers (in mature bamboo tissue), thin-walled vessels and sieve tubes, and parenchyma [7,10–12]. Mechanically, the structure resembles a fiber-reinforced composite, with the parenchyma acting as the matrix [13–17]. The sclerenchyma fibers typically have several layers, alternating between broad layers with low microfibril angle and narrow layers with high microfibril angle in the secondary wall [10]; the cellulose microfibrils are arranged such that the Young's modulus of the sclerenchyma fibers is much greater along the length of the fibers than in the transverse directions [18].

The parenchyma cells, serving as a matrix, are more thinly walled and lower density than the stiffer sclerenchyma fibers [7,19]. Dixon and Gibson measured a relative density of 0.22 for moso bamboo (*Phyllostachys pubescens*) parenchyma from SEM images [20], while Palombini et al. measured a relative density of 0.274 for parenchyma in *Bambusa tuldoides* with micro X-ray computed tomography (μ-CT) [21]. Note that relative density is the density of the cellular material, ρ^*, in this case the parenchyma, divided by that of the solid cell wall material, ρ_s. Ahvenainen et al. measured an average aspect ratio of the parenchyma cells

* Corresponding author.
E-mail address: ljgibson@mit.edu (L.J. Gibson).

https://doi.org/10.1016/j.actbio.2017.12.036
1742-7061/

of 1.6 with μ-CT [22]. SEM micrographs of the parenchyma are shown in Fig. 1. Additionally, the cellulose microfibrils in the parenchyma cell wall exhibit a substantially lower degree of orientation than those of the sclerenchyma fibers [22], suggesting that the parenchyma cell wall is roughly isotropic.

The sclerenchyma fibers of the vascular bundles have been the focus of a number of mechanics investigations, including a numerical investigation of the molecular bonding of their microfibrils [23], nanoindentation [18,24,25] and studies of single fiber tensile properties [12,24,26,27]. Bamboo parenchyma mechanics, however, is less well studied; investigations of the parenchyma properties are generally limited to nanoindentation measurements [17,18,28].

Models for the mechanical behavior of bamboo require an understanding of how the parenchyma properties depend on density. Bamboo parenchyma tissue is a cellular solid, with slightly elongated cells that stack in roughly vertical columns (Fig. 1). Cellular solids are generally thought of as either honeycomb-like (with two-dimensional prismatic cells) or foam-like (with three-dimensional polyhedral cells). Bamboo parenchyma is intermediate to these two cellular geometries: the short, closed cells, with some curvature in the cell walls, resemble a foam, while the roughly vertical stacking of the cells resembles a honeycomb. When loaded along the prism axis, honeycombs deform by uniaxial compression or stretching, and their longitudinal Young's moduli are linearly related to their relative density. When loaded perpendicular to the prism axis, they deform by bending, and their in-plane Young's moduli depend on the cube of their relative density [29]. Open-cell foams deform by bending; their Young's moduli depend on the square of their relative density. In closed-cell foams, the edges of the cells deform by bending while the faces stretch, so that their Young's moduli depend on relative density raised to a power between one and two [29]. From images of the structure of bamboo parenchyma, it is not clear which of these models and corresponding deformation modes is dominant.

Many plant tissues possess features that are small, soft and complex in their organization. It can be quite challenging to extract and mechanically test specific tissues (groups of similar cells). Moreover, one would ideally like to separate the contributions of the cell wall and the cellular geometry on plant tissue mechanics. Micro X-ray computed tomography (μ-CT) is a powerful tool for the visualization of plant structure, particularly its cellular architecture [30,31]. To date, this technique has been employed to understand the structure and properties of wood [32,33] as well as the structure of bamboo [21,22,34–36]. Importantly, one can also transform μ-CT imaging data into physical models using 3D printing, which has been well established in biomedical research [37], but is relatively unexplored for plant tissues.

3D printing has been used to explore the structure–property relationships in bioinspired and biological materials [38]. For example, Compton and Lewis printed honeycombs with composite cell walls consisting of silicon carbide and carbon fibers in epoxy [39], while Malek et al. developed finite element models of these balsa wood-inspired architectures [40]. Gladman et al. printed flower-like structures, composed of a composite hydrogel ink, that change shape with water uptake [41]. Denes 3D printed and mechanically tested highly-simplified cellular structures based on the structure of spruce for preliminary assessments of sandwich panel core material fabrication and suitability [42,43]. However, to date, the complex cellular structure of plant tissue has not yet been fully recapitulated and studied.

Here, we use 3D printing to fabricate models of bamboo parenchyma, based on μ-CT imaging using synchrotron radiation. Bamboo parenchyma is well suited to this approach due to the small regions between sclerenchyma fibers and its low stiffness. The objective of this study was to determine if bamboo parenchyma behaves more like a honeycomb or a foam in the linear elastic regime, based on the measured modulus-density relationship of the 3D printed models of bamboo parenchyma and cellular solids models for honeycombs and foams. We fabricated a series of 3D printed models of parenchyma with the same cellular geometry, but different relative densities, and then mechanically tested and compared them with models for foams and honeycombs. As a benchmark, we also printed and tested models of different cellular geometries with similar densities. We find that the parenchyma-based cellular structures behave like foams, deforming primarily by cell wall bending. Based on our observations, we also discuss the advancements needed for studying the mechanics of other biological materials using this approach.

2. Materials and methods

2.1. Materials

All materials came from a single internode of moso bamboo, obtained from the importer, Bamboo Craftsman Company (Portland, OR). Approximately 30 small matchstick specimens (long axis – longitudinal, approximate dimensions were 1.5 mm × 1.5 mm × 20 mm) were cut from the moso bamboo internode. Specimens were air-dry.

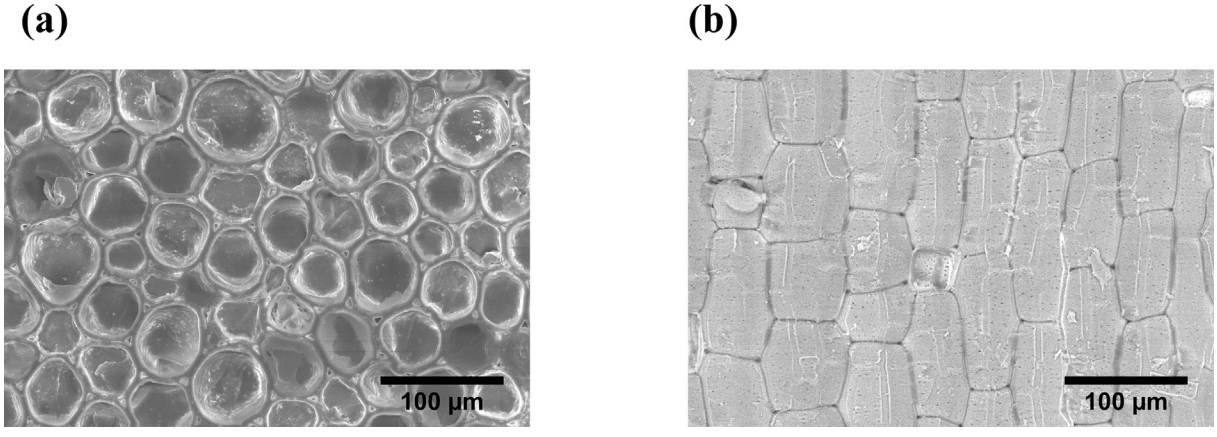

Fig. 1. SEM images of bamboo parenchyma. (a) Cross-sectional image; (b) longitudinal image.

Please cite this article in press as: P.G. Dixon et al., 3D printed structures for modeling the Young's modulus of bamboo parenchyma, Acta Biomater. (2018), https://doi.org/10.1016/j.actbio.2017.12.036

2.2. Micro X-ray computed tomography (μ-CT)

Micro-CT scans were performed on the specimens, using synchrotron radiation at the 2-BM-A beamline of the Advanced Photon Source (APS) at Argonne National Laboratory (Argonne, IL). An X-ray beam energy of 20.2 keV, a voxel size of 0.87^3 μm^3 (resolution = 1.74 μm, microfibrils and microfibril angle were not revealed by the tomography), a sample to detector distance of 90 mm, 1500 projections over 0° to 180°, and an exposure time of 100 ms were used. X-ray phase contrast was used to enhance the image contrast. The sample slice images were reconstructed with Tomopy, an open-source software package developed at the APS [44]. Phase retrieval [45] was applied to the projection images before the tomographic reconstruction. The gridrec algorithm was used for tomographic reconstruction [46], and the reconstructed slices were saved as floating-point images.

We initially planned to do high resolution microCT scanning at APS while loading bamboo specimens (consisting of nearly all parenchyma) longitudinally. Unfortunately, the appropriate deformation stage at APS was broken, so that we were unable to do deformation testing in the synchrotron. We deduced the deformation mechanism of bending from the modulus-density data and from models for cellular solids: for honeycombs loaded along the prism axis, modulus varies linearly with density while for open-cell foams, modulus varies with the square of density.

2.3. Image processing

Three individual reconstructed image stacks (from separate specimens and scans) were selected for printing based on their longitudinal alignment with the stack direction and the availability of relatively large regions parenchyma tissue. The reconstructed slices had to be processed so that the 3D printer software could read the files for printing. Two stereolithography (SLA) printers, an EnvisionTEC Perfactory MicroXL-Printer (Dearborn, MI, US) and a Formlabs Form 2 Printer (Somerville, MA), were used to fabricate the parenchyma tissue models. Due to problems with one of the printers, we were unable to use a single printer to fabricate all of the models. The EnvisionTEC printer was used to print three models based on parenchyma tissue in three different specimens of bamboo; each of which had a different cellular geometry, but roughly the same relative density. The Formlabs printer was used to fabricate models with the same cellular geometry, but different relative densities (Table 1). Two slightly different image processing methods were used to obtain the correct file formats required for each printer. In both cases, reconstructed slices were opened and processed as an image stack in ImageJ, an open-source image analysis program developed by the National Institutes of Health (https://imagej.nih.gov/ij/).

For the EnvisionTEC printer, image stacks from scans of three specimens with different cellular geometries were used; these are referred to as cellular geometries 1, 2 and 3 (Table 1). The relative densities of the specimens were similar (0.309–0.326). Regions, 684 pixels × 513 pixels, consisting of nearly all parenchyma (and only parenchyma in the central region) were selected and cropped from the stacks. The regions were then resized to 1024 pixels × 768 pixels with a bilinear interpolation, which changed the pixel size from 0.87 μm to 0.58 μm. However, the spacing between the stacks remained 0.87 μm. These stacks were then made binary (white/black) using the "Make Binary" operation with the "Default" threshold setting in ImageJ. Even with synchrotron radiation, segmenting the parenchyma cell walls from the air in lumens proved difficult. The binary method left some noise in the lumens, which was removed using the Particle Remover plugin with a size setting of 0–1000 $pixel^2$. The central region composed of 730 pixels × 730 pixels was selected and the cell walls were made white with a value of 255, and the voids were black with a value of 0. The stacks were saved as PNG image sequences. Each image was repeated three times in the print stack (with 50 μm thickness/slice in the z direction so that 0.87 μm → 150 μm in z), while each pixel was expanded to final dimensions of 0.58 μm → 97.58 μm in x–y. The relative densities of the cellular geometries, used for printing, were measured with the voxel counter plugin of ImageJ.

The models fabricated using the Formlabs printer all had the same cellular geometry (number 3, Table 1), and their relative density was varied by thickening or thinning the cell walls using image processing to yield relative densities of 0.326 (corresponding to the original scan), 0.362, 0.430 and 0.494. The higher relative densities are somewhat beyond the limit for Gibson and Asbhy's cellular solids models; it was not possible to fabricate models with lower relative densities due to image processing and printing issues, described below. The cropped images from the reconstructed slices were used; however, the images were not resized. The images were made binary and particles were removed using the same methods (particle size for removal scaled down, 0–446 $pixel^2$). Similarly, the center region (488 pixels × 488 pixels) was selected. These files were saved as a PNG image sequence, and then used to adjust the densities by dilating and then eroding the cell wall thickness. Images were first dilated by adding four pixels to each side of the wall, thickening the cell walls and closing small holes that were observed at the nodes of the cell walls. These images were then eroded by two pixels on each side of the cell wall and saved as a PNG sequence giving a relative density of 0.494. The image stack was eroded once more to give a relative density of 0.430 and yet

Table 1
Parenchyma print density and Young's modulus.

Printer	Print	Relative density, $(\rho^*/\rho_s)^+$	Young's modulus, E^* or E_s [MPa]
EnvisonTEC Perfactory MicroXL	Cellular Geometry No. 1	0.314	280.6 ± 8.2
	Cellular Geometry No. 3	0.309	228.0 ± 7.9
	Cellular Geometry No. 3	0.326	258.9 ± 11.0
	Solid	1.000	1855.3 ± 62.1 (n = 3)
Formlabs Form 2	Cellular Geometry No. 3	0.326	118.4 ± 6.2
	Cellular Geometry No. 3	0.326	131.0 ± 9.2
	Cellular Geometry No. 3	0.362	261.6 ± 17.5
	Cellular Geometry No. 3	0.362	296.3 ± 22.1
	Cellular Geometry No. 3	0.430	423.1 ± 33.8
	Cellular Geometry No. 3	0.430	469.3 ± 27.4
	Cellular Geometry No. 3	0.494	544.6 ± 32.5
	Cellular Geometry No. 3	0.494	656.0 ± 44.8
	Solid	1.000	1580.9 ± 72.2 (n = 4)

[+] Relative densities obtained from image stacks.

Please cite this article in press as: P.G. Dixon et al., 3D printed structures for modeling the Young's modulus of bamboo parenchyma, Acta Biomater. (2018), https://doi.org/10.1016/j.actbio.2017.12.036

again to give a relative density of 0.362. To create the STL files for the Formlabs printer, these stacks (the original, 0.326 relative density model, which preserved the holes at the nodes of the cell walls, and the density adjusted models) were opened and cropped to remove the boundary, and then the plugin BoneJ [47] was used with the isosurface command to create surfaces and save binary STL files. Lower density models of the cellular geometries, requiring further erosion of the cell walls, could not be created because of extensive connectivity issues formed by this cell wall thinning. The relative densities of the adjusted density image sequences of the cellular geometry were measured with the voxel counter plugin of ImageJ.

2.4. 3D printing

Three models, with three different cellular geometries, were printed directly from the prepared image stacks (described above) using the EnvisionTEC printer (EnvisionTEC Perfactory MicroXL-Printer) and HTM140 V2 resin (EnvisionTEC, Dearborn, MI, US). Sixteen 1024 pixel × 768 pixel fully filled (255 valued) PNG files were added to the beginning of the stack to support the print. Print resolution and scaling was noted above, but to clarify, the 1024 pixel × 768 pixel images map to 99.93 mm × 74.97 mm in real space. The maximum height permitted by this printer is 100 mm, allowing for 2000 images. This and the scale allowed for 662 individual slices to be fed into the printer, with the first parenchyma slice image printed only once and the remainder printed three times. The model volume of 99 mm × 71 mm × 71 mm corresponds to an actual parenchyma volume of 575 μm × 424 μm × 424 μm, giving a printed magnification of ~170×. Note the magnification in the z-axis is slightly higher (~3%) than either the *x*- or *y*-axes due to the slightly mismatched scales.

Build instructions were created in a text file by inspecting the build instructions of other simple print jobs. The build instructions were adjusted so that the first 34 images (including the support images), corresponding to the first 1.75 mm of the printed part, were printed with support settings to allow for easy part removal from the printer platen. Each build was then loaded into the EnvisionTEC Perfactory MicroXL printer's software. The print direction was through the stack, i.e., along the longitudinal direction of the structure. These large prints require considerable resin volumes (~200 mL); the print jobs were paused when the reservoir needed to be refilled. When the job finished, the model was removed and cleaned thoroughly with isopropanol followed by milling to remove the supporting base.

Duplicate prints of one bamboo specimen, cellular geometry no. 3, with adjustments for different densities, were fabricated with the Formlabs Form 2 printer. The STL files were loaded into Formlabs software, Preform, and then they were resized to 96 mm × 71 mm × 71 mm to achieve a similar magnification of ~170× in the prints. Support was generated without internal support, so that support material would not be printed inside the closed cells of the models. These specimens were printed with Formlabs Grey Resin V3 (GPGR03) at a layer thickness of 100 μm. When printing was completed, they were removed from the platen and cleaned with isopropanol. The support material was then removed manually followed by sanding to eliminate any protrusions on the faces to be loaded in compression. It should be noted that all parenchyma models fabricated by both printers contained some liquid resin entrapped within their closed cells.

Solid blocks (50 mm × 13 mm × 13 mm) of the two resins were printed using both printers to assess their Young's moduli. No post cure procedure was performed to avoid possible curing of liquid resin enclosed in the cellular structures and differential curing on such large parts. After printing, all specimens were stored in the dark.

2.5. Density and mechanical measurements

The density of all specimens was calculated from measurements of their overall dimensions (with calipers) and mass. The relative density was calculated by normalizing the measured densities of the printed parenchyma models by the average densities calculated from measurements of the solid blocks of the respective solid. The specimen density and relative density would be increased by any entrapped liquid resin.

All printed specimens were tested non-destructively in uniaxial compression, along the structure's longitudinal direction. We measured the compressive response of the model of the bamboo parenchyma, treating the model as a cellular material. Testing was done using an Instron 5566 test frame (Instron, Norwood, MA), equipped with a 10 kN load cell. Strain was measured by optical tracking. Six dot pairs were used as visual strain indicators and placed over the middle (approximately middle 60–70 mm) of one face of the printed parenchyma models, while three dot pairs were used on the solid blocks (middle 20–30 mm). Imaging was performed with either a Canon EOS 5D Mark III camera or a Canon EOS Rebel T2i camera with a Canon Macro Lens EF 100 mm 1:2.8 L (Melville, NY). Each parenchyma structure and solid block was tested three times at a crosshead speed of 0.0015 mm/s. For the EnvisonTEC parenchyma models and the corresponding solid blocks, maximum test stresses of 0.6 MPa and 8.6 MPa were used, respectively. The Formlabs parenchyma models were loaded to different maximum test stresses based on their relative density, from 0.7 MPa (for the two lowest relative density structures, that generated from original binary stack with a relative density of 0.326 and the 0.362 relative density structure) to 1.1 MPa (for the highest relative density structure). The corresponding solid blocks were loaded to a maximum test stress of 10.7 MPa. The load and optical deformation data were processed using Matlab (Mathworks, Natick, MA) to give stress-strain curves. A frame rate of 1/s was used to obtain the images for the strain measure. The first and last five images extracted from the videos were removed from the analysis, as the first few images may have contained noise from vibrations as result of starting to record and the last images may have been from video after the test was stopped. For each specimen, the Young's modulus was calculated based on the linear fit of the stress-strain curve from 25% to 85% of the maximum test stress.

3. Results

Fig. 2 is a visualization of the parenchyma tissue with images from cellular geometry no. 3. Fig. 2(a) shows a slice of an image stack obtained from μ-CT and cropped to consist of parenchyma only. Note the small holes at the nodes of the cell walls. The green outline shows the region selected for printing. Fig. 2(b) shows this same image but now processed for printing. The processed image was printed directly using the EnvisionTEC printer. The processed slices to construct the STL files used with the Formlabs printer look almost identical, but without surrounding background (and very slightly different as result of the different image size). A view of this STL file (corresponding to the original image stack, i.e. without erosion and dilation operations) is shown in Fig. 2(c) (view taken in Microsoft's 3D builder). Fig. 2(d) shows a longitudinal view of the processed image stack in Image J's Volume Viewer plugin. (This image is only for visualization purposes and was not used in printing; again note the small holes at the nodes of the cell walls.) Photographs of the printed structures are displayed in Fig. 3. Models from both printers captured the cellular geometry of the bamboo parenchyma quite well.

For the EnvisionTEC models (scans of different bamboo specimens, with different cellular geometries and roughly constant

Please cite this article in press as: P.G. Dixon et al., 3D printed structures for modeling the Young's modulus of bamboo parenchyma, Acta Biomater. (2018), https://doi.org/10.1016/j.actbio.2017.12.036

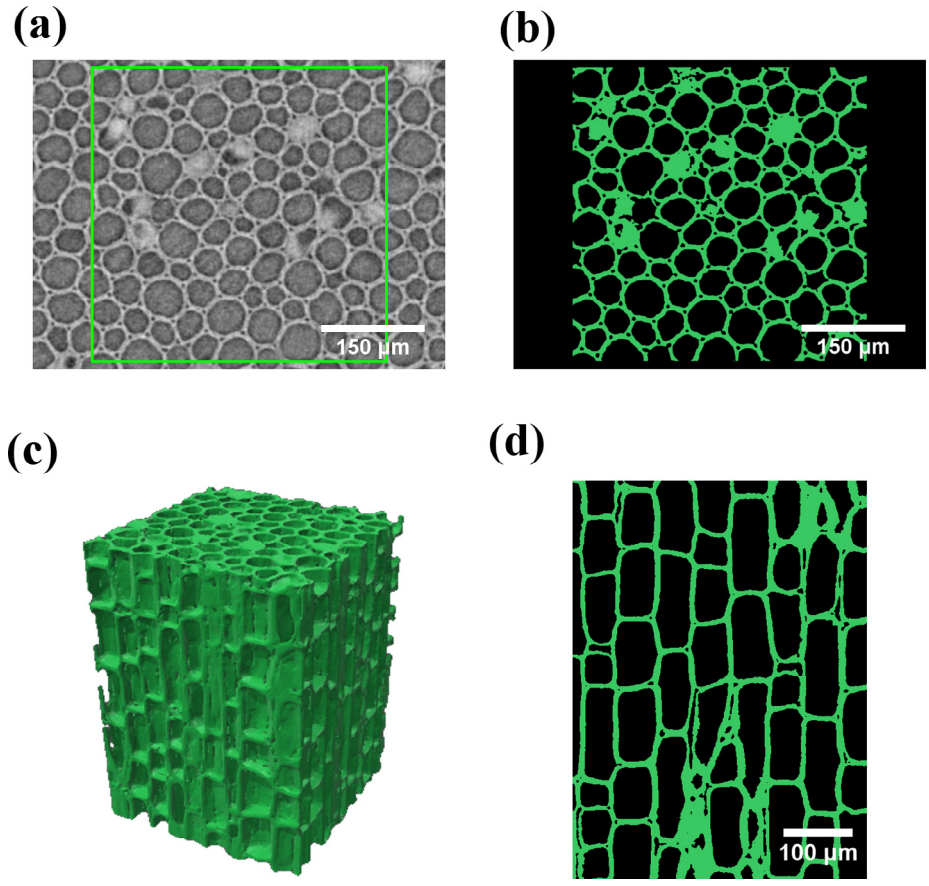

Fig. 2. Visualization of the parenchyma tissue from cellular geometry no. 3. (a) Shows a μ-CT slice of an image stack. Note the small pores in the nodes of the cell walls. (b) Is the same image but now processed for printing. (c) Shows a view of the STL file created from the image stacks corresponding to the unaltered processed geometry (i.e. without erosion and dilation operations). The short edges are 425 μm and 71 mm in the tissue and print, respectively. (d) Shows a longitudinal view of the processed image stack.

relative density), the average relative density calculated from the processed images was 0.316 ± 0.009 (mean ± standard deviation). The unaltered images (no erosion or dilation applied) used for STL construction (cellular geometry 3, for Formlabs prints) gave a relative density of 0.326, the same as that for the images printed directly in the EnvisionTEC model, as expected. Densities measured for the two solid blocks were 1191 kg/m^3 and 1162 kg/m^3, for the HTM 140 V2 and Grey Resin V3, respectively. For the EnvisionTEC structures, the measured densities and corresponding relative densities, 0.395 ± 0.024 (mean ± standard deviation), were roughly 25% higher than the relative densities obtained from the images. For the Formlabs structures, the measured densities and corresponding relative densities were nearly 20% higher than the relative densities obtained from the images (0.524 ± 0.075 vs. 0.429 ± 0.059, mean ± standard deviation) with the exception of the 0.326 relative density models, which were nearly same as those obtained in the images (0.326 vs. 0.329). This difference is primarily attributed to some liquid resin entrapped in the closed cells in the prints, observed when cutting open a model from each printer (see SI Fig. S1 in SI). This is not observed in the 0.326 relative density set of Formlabs structures, as there are connectivity issues due to the inherent challenges associated with STL mesh generation. The resulting small gaps and holes in the cell walls allow for the trapped resin to flow out.

Fig. 4 shows a stress-strain curve from a compression test on a Formlabs parenchyma model (relative density of 0.362). The Young's modulus for each model is shown in Table 1. Note the standard deviations of the parenchyma print results are for the repeated tests of the same specimen. In the case of the Young's moduli of the solid blocks, the standard deviations are for tests on multiple samples, listed in parentheses as n. The Young's moduli of the parenchyma models, E^*, normalized by that of the solid wall (i.e., the resin), E_s, ranges from 0.07 to 0.42 for relative densities between 0.3 and 0.5 (Fig. 5) (this normalization accounts for the different resins), and demonstrates power law scaling according to Eq. (1).

$$(E^*/E_s) = 1.979(\rho^*/\rho_s)^{2.333} \quad r^2 = 0.956 \quad n = 9 \tag{1}$$

All data is included in the fit except for that obtained from the two 0.326 relative density Formlabs prints, which were excluded due to connectivity issues (Section 4.1).

4. Discussion

Mechanical testing of models of biological tissues made by 3D printing, based on μ-CT imaging of those tissues, has potential for increasing our understanding of their mechanical behavior. The method allows the three-dimensional nature of tissues to be captured and enables mechanical testing of larger specimens than would be possible from the available tissue. The low degree of orientation of the microfibrils in the cell walls of moso bamboo parenchyma [22] suggests that the cell wall is roughly isotropic, like the resin used to print the models [48]. While the solid cell wall properties of the parenchyma and resin differ, for isotropic

Please cite this article in press as: P.G. Dixon et al., 3D printed structures for modeling the Young's modulus of bamboo parenchyma, Acta Biomater. (2018), https://doi.org/10.1016/j.actbio.2017.12.036

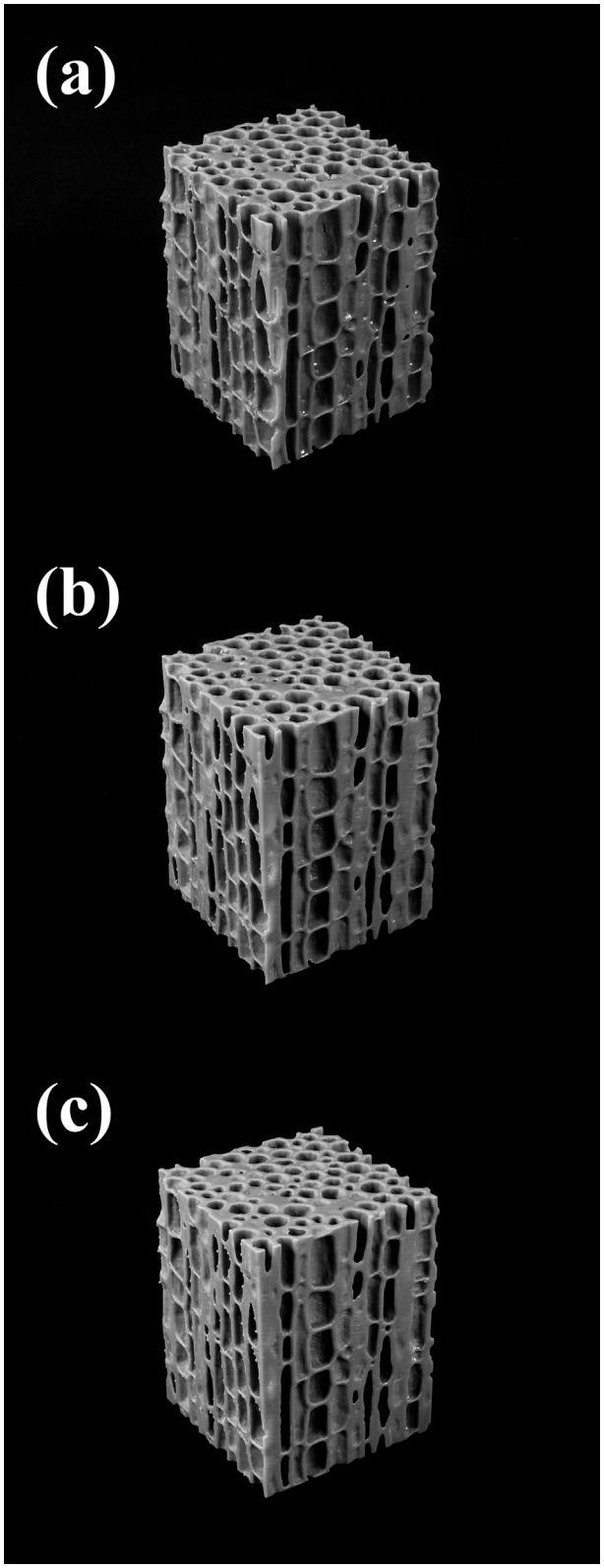

Fig. 3. Photographs of Formlabs parenchyma models, with relative densities of (a) 0.362, (b) 0.430, and (c) 0.494. Short edges are 71 mm (vary slightly with density), and long edges are 96 mm.

materials, we expect the same elastic deformation mechanism in the model materials and the moso bamboo parenchyma.

Our method allows study of the behavior of the effect of a tissue's cellular geometry on its mechanical behavior, independent of that of a complex cell wall. This may be useful in the validation

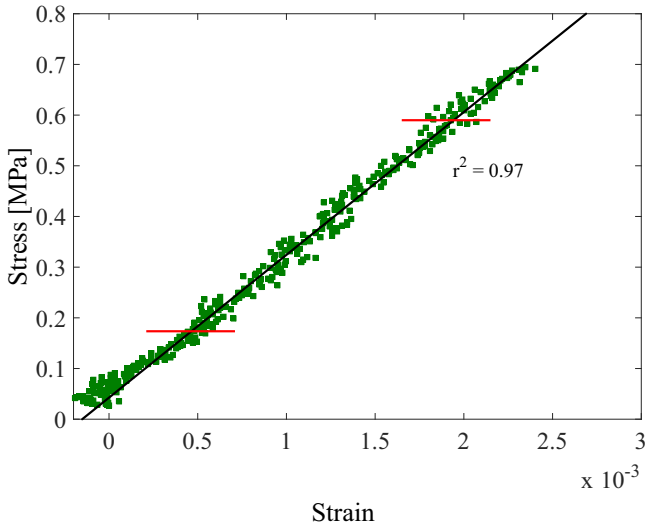

Fig. 4. The compressive stress strain curve of a Formlabs Form 2 cellular geometry 3 parenchyma model (relative density 0.362). The Young's modulus is obtained from the best fit line through the data between 25% and 85% of the maximum stress.

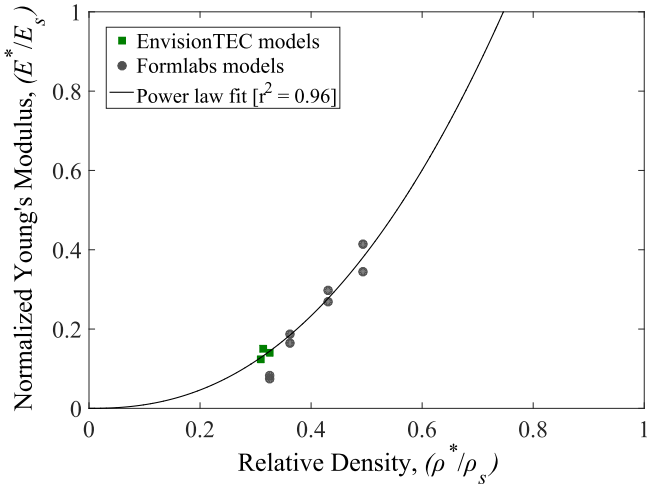

Fig. 5. Normalized Young's modulus plotted against relative density (measured from images of the stack).

of numerical models for the mechanical behavior of plant tissues. Models created and tested with this method ideally could be used to verify a numerical model of a tissue's structure, before applying complex tissue cell wall properties in the model. Aimene and Nairn performed work along these lines in a two dimensional case, considering the transverse compression of wood [49]. They created material point method models from SEM cross-sectional micrographs of wood and first verified the model with deformation from simplified polyoxymethylene model capturing the wood tissue anatomy [49]. The method of this current work could extend studies like that of Aimene and Nairn [49] to capture tissue structure in three dimensions in model fabrication. Similarly, this method could be used with mechanical testing of both the tissue and the cell walls to aid interpretation of the results, given the difficulties and limitations of micro-mechanical test methods [50–52]. While promising, the combined method of μ-CT imaging and 3D printing needs further development for it to be truly deployed in this way and there are key limitations inherent to this approach, described in more detail in Section 4.2.

Please cite this article in press as: P.G. Dixon et al., 3D printed structures for modeling the Young's modulus of bamboo parenchyma, Acta Biomater. (2018), https://doi.org/10.1016/j.actbio.2017.12.036

4.1. Normalized Young's moduli

The compression tests on the models of bamboo parenchyma indicate that their relative Young's moduli vary with relative density raised to the power 2.33, suggesting that bending of the cell walls is the dominant mechanism of deformation [29,53]. For an ideal open-cell foam (isotropic and with relative densities below 0.3), models indicate that the relative modulus varies with relative density squared [29]. We note that the relative densities of the models in this study were somewhat higher than the upper limit of 0.3 for modeling an ideal foam; however, a squared dependence of modulus on density has been observed in foams at higher densities [29]. An exponent of two is often the largest observed for closed-cell foams [54]. However, closed-cell metallic foams often exhibit open-cell foam mechanical behavior if there is curvature in the cell walls [55]; in this study, the exponent is slightly larger than two. Moso bamboo parenchyma cells, too, have some curvature in the cell walls (Figs. 1, 2). The exponent slightly above two may also be a result of the high range of relative density of the specimens or increased connectivity at higher densities (limitations are discussed in more detail in Section 4.2).

For ideal open-cell foams, the constant in the Young's modulus-density relationship depends on the cellular geometry; for many foams, the constant is one. The value of 1.979 found here for moso bamboo parenchyma is not surprising, given the box-like shape of the cells and the cell aspect ratio of 1.6 [22].

The Formlabs parenchyma structures with a relative density of 0.326 have considerably lower normalized Young's moduli than the EnvisionTEC models (Fig. 5). This unexpected ~40% reduction is a result of the different printing methods. STL generation leads to some information loss. In the case of the original image stack (no erode or dilate operations applied), small gaps and holes in the cell walls, leading to connectivity issues, not seen to such a degree in the other prints, are visible (see SI Fig. S2). It is hypothesized that these defects result in lower measured normalized Young's moduli. While STL generation from images likely allows for a wider variety of 3D printers to be used more easily, it is less direct. For future work, 3D printing directly from images is recommended to avoid these defects.

4.2. Limitations and opportunities

Aspects of the specific method used in this study limit the interpretation of the results. These limitations pertain to the structure of printed parenchyma models and stem from a variety of sources. Limitations associated primarily with imaging and image processing will be discussed first. The relative density range of the test specimens is limited and their absolute values exceed 0.3. It was initially planned to test lower densities, but the images, and, to a greater degree the generated STL files, had cell wall connectivity issues that required the images to be dilated to remove the holes at nodes of the cell walls. It should also be noted that the binary operation did not result in all cell walls being completely connected. There were rare instances in the cell wall where the grey value was considerably lower and thresholded as background. These instances were not corrected, as they may correspond to physical regions of the actual cell wall with much lower stiffness and poorer load transfer capability. In higher density structures, some of these areas may become solid cell wall, resulting in stiffness increases due to increased connectivity and higher density.

Similar limitations are associated with the tissue itself and printing. In the tissue, regions of parenchyma are interrupted by vascular bundles, limiting the number of cells in a cross section. The printer build volumes and required magnification to print high fidelity structures and to avoid filling the cells completely with entrapped resin, similarly limit the number of cells along the longitudinal direction. Our printed structures are roughly 8 cells × 8 cells × 6 cells (Fig. 2), roughly approaching the number needed to treat the cellular material as a continuum [55,56]. Liquid resin entrapped in the cells increases the relative density of the printed parenchyma models, compared with that measured from the images. Partially filling the lumen of the cells with liquid does not affect the mechanical response; Warner et al. demonstrate that partially filled closed-cell foams show a bending dominated response (like that of dry foams) [57]. Note that if a liquid fully fills the lumens, then the incompressibility of the liquid does contribute to the mechanical response of a closed-cell foam. Given that the measured densities indicate that liquid only partially filled cells, and the small strains (and thus volume changes) imposed during mechanical testing, it is highly unlikely that liquid resin considerably alters the mechanical response.

The resolution of commercial SLA printers is on the order of 100 μm, and build volumes are on the order of a million mm^3 (as is the case with the printers used in this study) [58–60]. This allows small features of tissues to be captured within enlarged models (for example, in this study, with the enlargement of ~170×, the holes at the cell wall nodes, on the length scale of 5 μm, were captured in printing with the EnvisionTEC printer, SI Fig. S3 shows this). Printing high fidelity models of tissue at the actual scale is not yet realizable with this method. Thus, the required scaling is an inherent limitation of this method. Similar to this limitation, μ-CT has a tradeoff between magnification and scanned volume [30]. Here, this was not limiting as the parenchyma tissue sampling was constrained by the presence of vascular bundles rather than the field of view (1.9 mm × 2.2 mm × 2.2 mm, with 0.87^3 μm^3 voxel size), but it is expected this could be an issue for some tissues. Advancements in SLA printing and μ-CT should lessen these inherent limitations.

An additional major limitation is the print material; actual solid cell walls of tissue are likely more complex than the SLA printed polymers. Polymers produced by stereolithography are generally homogenous and isotropic [48]. As explained previously, the low degree of orientation of cellulose fibrils in the parenchyma cell wall [22], substantially lessens this problem for the current study. However, the solid cell wall of actual tissues is often more complex; for instance, plant cell walls are often highly oriented fiber composites [29].

With more advanced additive manufacturing techniques, this method could better capture the complex nature of biological cell walls. Multi-material techniques, [61], could allow for the construction of more complex models. Recently, fiber reinforced 3D printing inks for ink-writing have been developed [39,40]. Additionally, advanced SLA printers, similar to that described in the work of Martin et al. [62] could be used allowing for reinforcement in the printed material. It is possible (likely even) that in the future, the fiber composite nature of plant cell walls could be captured in 3D printed models of plant tissues. Oxman et al. noted that work is being performed in the field of light-based 3D printing to incorporate mechanical property gradients into a printed solid [63]. As the printable solids become more advanced and allow better capture of the cell wall structure in nature, the possibility of an approach combined with μ-CT to capture the cellular structure presents interesting possibilities.

5. Conclusions

An integrated approach that combines 3D printing and imaging was developed to aid in the understanding of plant tissue structure-property relationships. Specifically, physical models of the cellular geometry of bamboo parenchyma were created by stereolithography using μ-CT images. The dependence of the longitudinal Young's modulus of these printed structures on relative

Please cite this article in press as: P.G. Dixon et al., 3D printed structures for modeling the Young's modulus of bamboo parenchyma, Acta Biomater. (2018), https://doi.org/10.1016/j.actbio.2017.12.036

density is well described with an exponent somewhat above 2. Our findings suggest that the parenchyma behaves like a foam, whose cell walls deform primarily by bending. As the resolution for these 3D printing and μ-CT imaging methods increases further, we anticipate that this integrated approach will provide even greater insights into the behavior of plant architectures, especially when validated by numerical models.

Acknowledgements

This research used resources of the Advanced Photon Source, a U.S. Department of Energy (DOE) Office of Science User Facility operated for the DOE Office of Science by Argonne National Laboratory under Contract No. DE-AC02-06CH11357. This work was enabled by preliminary work performed in part at the Center for Nanoscale Systems (CNS), a member of the National Nanotechnology Infrastructure Network (NNIN), which is supported by the National Science Foundation under NSF award no. ECS-0335765. CNS is part of Harvard University. The authors also thank: Greg Lin for help with preliminary μ-CT scans of bamboo, Emeric Plancher and Cem Tasan for access to computational facilities; James Hunter and Mike Tarkanian for help with machining and the Form 2 printer; and Lori Sanders for photography.

Funding

This paper is based upon work supported by the National Science Foundation under OISE: 1258574. The views expressed in this paper are not endorsed by the National Science Foundation. Additionally, this work was also supported by BASF through the North American Center for Research on Advanced Materials and the Martin Family Society of Fellows for Sustainability. The work carried out in the Lewis Lab was supported by National Science Foundation, Grant DMR-1305284 and the Vannevar Bush Faculty Fellowship Program sponsored by the Basic Research Office the Assistant Secretary of Defense for Research and Engineering and funded by the Office of Naval Research Grant N00014-16-1-2823.

Disclosure

MA Skylar-Scott owns stock of Formlabs Inc. JA Lewis is a co-founder of Voxel8, Inc, which focuses on multi-material 3D printing. The other authors have no conflicts of interest.

Appendix A. Supplementary data

Supplementary data associated with this article can be found, in the online version, at https://doi.org/10.1016/j.actbio.2017.12.036.

References

[1] Global Forest Resources Assessment 2010, Food and Agriculture Organization of the United Nations (FAO), Rome, 2010.
[2] D. Nayyar, China, India, Brazil and South Africa in the World Economy: Engines for Growth?, UNU-WIDER, Helsinki, 2008
[3] Z. Jiang, Bamboo and Rattan in the World, China Forestry Publishing House, Beijing, China, 2007.
[4] S. Lucas, Bamboo, Reaktion Books LTD, London, U.K., 2013.
[5] J. Vogtländer, P. van der Lugt, H. Brezet, The sustainability of bamboo products for local and Western European applications. LCAs and land-use, J. Clean. Prod. 18 (2010) 1260–1269, https://doi.org/10.1016/j.jclepro.2010.04.015.
[6] B. Sharma, A. Gatoo, M. Bock, H. Mulligan, M. Ramage, Engineered bamboo: state of the art, Proc. ICE Constr. Mater. 168 (2015) 57–67, https://doi.org/10.1680/coma.14.00020.
[7] W. Liese, Research on bamboo, Wood Sci. Technol. 21 (1987) 189–209.
[8] E. Sjöström, Wood Chemistry: Fundamentals and Applications, 2nd ed., Academic Press, San Diego, 1993.
[9] U.G.K. Wegst, Bending efficiency through property gradients in bamboo, palm, and wood-based composites, J. Mech. Behav. Biomed. Mater. 4 (2011) 744–755, https://doi.org/10.1016/j.jmbbm.2011.02.013.
[10] N. Parameswaran, W. Liese, On the fine structure of bamboo fibres, Wood Sci. Technol. 10 (1976) 231–246.
[11] C.S. Gritsch, G. Kleist, R.J. Murphy, Developmental changes in cell wall structure of phloem fibres of the bamboo *Dendrocalamus asper*, Ann. Bot. 94 (2004) 497–505, https://doi.org/10.1093/aob/mch169.
[12] Y. Yu, H. Wang, F. Lu, G. Tian, J. Lin, Bamboo fibers for composite applications: a mechanical and morphological investigation, J. Mater. Sci. 49 (2014) 2559–2566, https://doi.org/10.1007/s10853-013-7951-z.
[13] F. Nogata, H. Takahashi, Intelligent functionally graded material: bamboo, Compos. Eng. 5 (1995) 743–751, https://doi.org/10.1016/0961-9526(95)00037-N.
[14] S. Amada, Y. Ichikawa, T. Munekata, Y. Nagase, H. Shimizu, Fiber texture and mechanical graded structure of bamboo, Compos. Part B Eng. 28B (1997) 13–20, https://doi.org/10.1016/S1359-8368(96)00020-0.
[15] Z.-P. Shao, C.-H. Fang, S.-X. Huang, G.-L. Tian, Tensile properties of Moso bamboo (*Phyllostachys pubescens*) and its components with respect to its fiber-reinforced composite structure, Wood Sci. Technol. 44 (2010) 655–666, https://doi.org/10.1007/s00226-009-0290-1.
[16] H. Liu, Z. Jiang, X. Zhang, X. Liu, Z. Sun, Effect of fiber on tensile properties of moso bamboo, BioResources 9 (2014) 6888–6898.
[17] M.K. Habibi, A.T. Samaei, B. Gheshlaghi, J. Lu, Y. Lu, Asymmetric flexural behavior from bamboo's functionally graded hierarchical structure: underlying mechanisms, Acta Biomater. 16 (2015) 178–186, https://doi.org/10.1016/j.actbio.2015.01.038.
[18] Y. Yu, B. Fei, B. Zhang, X. Yu, Cell-wall mechanical properties of bamboo investigated by in-situ imaging nanoindentation, Wood Fiber Sci. 39 (2007) 527–535.
[19] D. Grosser, W. Liese, On the anatomy of Asian bamboos, with special reference to their vascular bundles, Wood Sci. Technol. 5 (1971) 290–312, https://doi.org/10.1007/BF00365061.
[20] P.G. Dixon, L.J. Gibson, The structure and mechanics of Moso bamboo material, J. R. Soc. Interface 11 (2014) 20140321, https://doi.org/10.1098/rsif.2014.0321.
[21] F.L. Palombini, W. Kindlein, B.F. de Oliveira, J.E. de Araujo Mariath, Bionics and design: 3D microstructural characterization and numerical analysis of bamboo based on X-ray microtomography, Mater. Charact. 120 (2016) 357–368, https://doi.org/10.1016/j.matchar.2016.09.022.
[22] P. Ahvenainen, P.G. Dixon, A. Kallonen, H. Suhonen, L.J. Gibson, K. Svedström, Spatially-localized bench-top X-ray scattering reveals tissue-specific microfibril orientation in Moso bamboo, Plant Methods 13 (2017), https://doi.org/10.1186/s13007-016-0155-1.
[23] S. Youssefian, N. Rahbar, molecular origin of strength and stiffness in bamboo fibrils, Sci. Rep. 5 (2015) 11116, https://doi.org/10.1038/srep11116.
[24] Y. Yu, G. Tian, H. Wang, B. Fei, G. Wang, Mechanical characterization of single bamboo fibers with nanoindentation and microtensile technique, Holzforschung 65 (2011) 113–119, https://doi.org/10.1515/HF.2011.009.
[25] X. Yang, G. Tian, L. Shang, H. Lv, S. Yang, X. 'e Liu, Variation in the cell wall mechanical properties of *Dendrocalamus farinosus* bamboo by nanoindentation, BioResources 9 (2014) 2289–2298.
[26] H. Yan-hui, F. Ben-hua, Y. Yan, Z. Rong-jun, Plant age effect on mechanical properties of moso bamboo (*Phyllostachys heterocycla var. Pubescens*) single fibers, Wood Fiber Sci. 44 (2012) 196–201.
[27] X. Wang, T. Keplinger, N. Gierlinger, I. Burgert, Plant material features responsible for bamboo's excellent mechanical performance: a comparison of tensile properties of bamboo and spruce at the tissue, fibre and cell wall levels, Ann. Bot. 114 (2014) 1627–1635, https://doi.org/10.1093/aob/mcu180.
[28] M.K. Habibi, L. Tam, D. Lau, Y. Lu, Viscoelastic damping behavior of structural bamboo material and its microstructural origins, Mech. Mater. 97 (2016) 184–198, https://doi.org/10.1016/j.mechmat.2016.03.002.
[29] L.J. Gibson, M.F. Ashby, Cellular Solids: Structure and Properties, 2nd ed., Cambridge University Press, Cambridge, UK, 1997.
[30] S. Dhondt, H. Vanhaeren, D. Van Loo, V. Cnudde, D. Inzé, Plant structure visualization by high-resolution X-ray computed tomography, Trends Plant Sci. 15 (2010) 419–422, https://doi.org/10.1016/j.tplants.2010.05.002.
[31] C.R. Brodersen, A.B. Roddy, New frontiers in the three-dimensional visualization of plant structure and function, Am. J. Bot. 103 (2016) 184–188, https://doi.org/10.3732/ajb.1500532.
[32] K. Steppe, V. Cnudde, C. Girard, R. Lemeur, J.-P. Cnudde, P. Jacobs, Use of X-ray computed microtomography for non-invasive determination of wood anatomical characteristics, J. Struct. Biol. 148 (2004) 11–21, https://doi.org/10.1016/j.jsb.2004.05.001.
[33] F. Forsberg, R. Mooser, M. Arnold, E. Hack, P. Wyss, 3D micro-scale deformations of wood in bending: synchrotron radiation μCT data analyzed with digital volume correlation, J. Struct. Biol. 164 (2008) 255–262, https://doi.org/10.1016/j.jsb.2008.08.004.
[34] G. Peng, Z. Jiang, X. Liu, B. Fei, S. Yang, D. Qin, H. Ren, Y. Yu, H. Xie, Detection of complex vascular system in bamboo node by X-ray μCT imaging technique, Holzforschung 68 (2014), https://doi.org/10.1515/hf-2013-0080.
[35] P. Huang, W.-S. Chang, M.P. Ansell, Y.M.J. Chew, A. Shea, Density distribution profile for internodes and nodes of *Phyllostachys edulis* (Moso bamboo) by computer tomography scanning, Constr. Build. Mater. 93 (2015) 197–204, https://doi.org/10.1016/j.conbuildmat.2015.05.120.
[36] J.Q. Krause, F. de Andrade Silva, K. Ghavami, O. da, F.M. Gomes, R.D.T. Filho, On the influence of *Dendrocalamus giganteus* bamboo microstructure on its

mechanical behavior, Constr. Build. Mater. 127 (2016) 199–209, https://doi.org/10.1016/j.conbuildmat.2016.09.104.
[37] F. Rengier, A. Mehndiratta, H. von Tengg-Kobligk, C.M. Zechmann, R. Unterhinninghofen, H.-U. Kauczor, F.L. Giesel, 3D printing based on imaging data: review of medical applications, Int. J. Comput. Assist. Radiol. Surg. 5 (2010) 335–341, https://doi.org/10.1007/s11548-010-0476-x.
[38] A.R. Studart, Additive manufacturing of biologically-inspired materials, Chem. Soc. Rev. 45 (2016) 359–376, https://doi.org/10.1039/C5CS00836K.
[39] B.G. Compton, J.A. Lewis, 3D-printing of lightweight cellular composites, Adv. Mater. 26 (2014) 5930–5935, https://doi.org/10.1002/adma.201401804.
[40] S. Malek, J.R. Raney, J.A. Lewis, L.J. Gibson, Lightweight 3D cellular composites inspired by balsa, Bioinspir. Biomim. 12 (2017) 26014, https://doi.org/10.1088/1748-3190/aa6028.
[41] A. Sydney Gladman, E.A. Matsumoto, R.G. Nuzzo, L. Mahadevan, J.A. Lewis, Biomimetic 4D printing, Nat. Mater. 15 (2016) 413–418, https://doi.org/10.1038/nmat4544.
[42] L. Denes, Hierarchical PLA structures used for wooden sandwich panel's core fortification, in: Proc 58th Int. Conv. Soc Wood Sci Technol, Jackson Hole, WY, USA, 2015, p. 544.
[43] L. Denes, Hierarchical PLA structures used for wooden sandwich panel's core fortification, (2015). http://www.swst.org/meetings/AM15/pdfs/presentations/denes.pdf (accessed 30.03.17).
[44] D. Gürsoy, F. De Carlo, X. Xiao, C. Jacobsen, TomoPy: a framework for the analysis of synchrotron tomographic data, J. Synchrotron Radiat. 21 (2014) 1188–1193, https://doi.org/10.1107/S1600577514013939.
[45] D. Paganin, S.C. Mayo, T.E. Gureyev, P.R. Miller, S.W. Wilkins, Simultaneous phase and amplitude extraction from a single defocused image of a homogeneous object, J. Microsc. 206 (2002) 33–40, https://doi.org/10.1046/j.1365-2818.2002.01010.x.
[46] B.A. Dowd, G.H. Campbell, R.B. Marr, V.V. Nagarkar, S.V. Tipnis, L. Axe, D.P. Siddons, Developments in synchrotron X-ray computed microtomography at the National Synchrotron Light Source, in: SPIEs Int. Symp. Opt. Sci. Eng. Instrum. International Society for Optics and Photonics, 1999, pp. 224–236.
[47] M. Doube, M.M. Kłosowski, I. Arganda-Carreras, F.P. Cordelières, R.P. Dougherty, J.S. Jackson, B. Schmid, J.R. Hutchinson, S.J. Shefelbine, BoneJ: free and extensible bone image analysis in ImageJ, Bone 47 (2010) 1076–1079, https://doi.org/10.1016/j.bone.2010.08.023.
[48] R. Hague, S. Mansour, N. Saleh, R. Harris, Materials analysis of stereolithography resins for use in rapid manufacturing, J. Mater. Sci. 39 (2004) 2457–2464, https://doi.org/10.1023/B:JMSC.0000020010.73768.4a.
[49] Y.E. Aimene, J.A. Nairn, Simulation of transverse wood compression using a large-deformation, hyperelastic–plastic material model, Wood Sci. Technol. 49 (2015) 21–39, https://doi.org/10.1007/s00226-014-0676-6.
[50] I. Burgert, Exploring the micromechanical design of plant cell walls, Am. J. Bot. 93 (2006) 1391–1401, https://doi.org/10.3732/ajb.93.10.1391.
[51] M. Eder, O. Arnould, J.W.C. Dunlop, J. Hornatowska, L. Salmén, Experimental micromechanical characterisation of wood cell walls, Wood Sci. Technol. 47 (2013) 163–182, https://doi.org/10.1007/s00226-012-0515-6.
[52] E.K. Gamstedt, T.K. Bader, K. de Borst, Mixed numerical–experimental methods in wood micromechanics, Wood Sci. Technol. 47 (2013) 183–202, https://doi.org/10.1007/s00226-012-0519-2.
[53] N.A. Fleck, V.S. Deshpande, M.F. Ashby, Micro-architectured materials: past, present and future, Proc. R. Soc. Math. Phys. Eng. Sci. 466 (2010) 2495–2516, https://doi.org/10.1098/rspa.2010.0215.
[54] A.P. Roberts, E.J. Garboczi, Elastic moduli of model random three-dimensional closed-cell cellular solids, Acta Mater. 49 (2001) 189–197, https://doi.org/10.1016/S1359-6454(00)00314-1.
[55] L.J. Gibson, Mechanical behavior of metallic foams, Annu. Rev. Mater. Sci. 30 (2000) 191–227, https://doi.org/10.1146/annurev.matsci.30.1.191.
[56] E.W. Andrews, G. Gioux, P. Onck, L.J. Gibson, Size effects in ductile cellular solids. Part II: experimental results, Int. J. Mech. Sci. 43 (2001) 701–713, https://doi.org/10.1016/S0020-7403(00)00043-6.
[57] M. Warner, B.L. Thiel, A.M. Donald, The elasticity and failure of fluid-filled cellular solids: theory and experiment, Proc. Natl. Acad. Sci. 97 (2000) 1370–1375, https://doi.org/10.1073/pnas.020501797.
[58] EnvisionTEC, Inc., Micro Plus Advantage | Desktop 3D Printer | EnvisionTEC, Micro Plus Advant. Deskt. 3D Print. EnvisionTEC. (not given). https://envisiontec.com/3d-printers/desktop-3d-printers/micro-plus-advantage/ (accessed 30.03.17).
[59] EnvisionTEC, Inc., Micro Plus XL | Desktop 3D Printer | EnvisionTEC, Micro Plus XL Deskt. 3D Print. EnvisionTEC. (not given). https://envisiontec.com/3d-printers/desktop-3d-printers/micro-xl/ (accessed 30.03.17).
[60] Formlabs, Inc., Desktop SLA 3D Printing Technical Specifications - Formlabs, Deskt. SLA 3D Print. Tech. Specif. – Formlabs. (2017). https://formlabs.com/3d-printers/tech-specs/ (accessed 30.03.2017).
[61] H.Z. Yu, S.R. Cross, C.A. Schuh, Mesostructure optimization in multi-material additive manufacturing: a theoretical perspective, J. Mater. Sci. 52 (2017) 4288–4298, https://doi.org/10.1007/s10853-017-0753-y.
[62] J.J. Martin, B.E. Fiore, R.M. Erb, Designing bioinspired composite reinforcement architectures via 3D magnetic printing, Nat. Commun. 6 (2015) 8641, https://doi.org/10.1038/ncomms9641.
[63] N. Oxman, S. Keating, E. Tsai, Functionally graded rapid prototyping, in: Innov. Dev. Virtual Phys. Prototyp. Proc. 5th Int. Conf. Adv. Res. Virtual Rapid Prototyp., Leiria, Portugal, 2011, pp. 483–490.

Please cite this article in press as: P.G. Dixon et al., 3D printed structures for modeling the Young's modulus of bamboo parenchyma, Acta Biomater. (2018), https://doi.org/10.1016/j.actbio.2017.12.036